IEEE Access
Multidisciplinary | Rapid Review | Open Access Journal

Received 1 June 2024, accepted 13 June 2024, date of publication 17 June 2024, date of current version 24 June 2024.

Digital Object Identifier 10.1109/ACCESS.2024.3415956

RESEARCH ARTICLE

Efficient Road Traffic Estimation for Proactive Beam Allocation in an ISAC Setup

WESAM AL AMIRI[1], (Member, IEEE), TERRY N. GUO[2], (Senior Member, IEEE), AND ALLEN B. MACKENZIE[1], (Senior Member, IEEE)

[1]Department of Electrical and Computer Engineering, Tennessee Technological University, Cookeville, TN 38505, USA

[2]Center for Manufacturing Research, Tennessee Technological University, Cookeville, TN 38505, USA Corresponding author: Wesam Al Amiri (waalamiri42@tntech.edu)

This work was supported by the National Science Foundation under Grant #2135275.

ABSTRACT Building efficient and effective road traffic monitoring systems has become a major challenge in different countries, mainly due to the rapid growth of the metropolis road network and the booming of vehicles. Existing traffic monitoring methods are accurate but typically come with inherent limitations, prompting the exploration of alternative techniques. Integrated sensing and communication (ISAC) offers an effective approach to traffic monitoring by leveraging the synergy between sensing and communication to enhance system efficiency and reduce costs. In this paper, we present a particular ISAC use case tailored for radio-based traffic monitoring. Both traffic density and speed estimations take advantage of communication functionality, involving the reuse of communication waveforms for the sensing purpose. In particular, proactive millimeter-wave (mmWave) beam allocation aided by traffic density estimation is studied to enhance communication coverage of vehicular users in the area of interest for bandwidth-intensive applications. Specifically, we exploit orthogonal frequency division multiplexing (OFDM) communication signals of opportunity reflected from targets (vehicles) to efficiently estimate the road traffic density and speed in a road section. A hybrid scheme combining model-based and data-driven methods is considered to build efficient estimators that require reduced-size training data and are less computationally complex.

Simulationandcomparisonresultsdemonstratethattheproposedtrafficestimationtechniquescanaccurately handle a wide range of numbers of vehicles, even with a small-sized dataset. Furthermore, the proactive beam allocation analysis shows that the quality of service (QoS, in terms of outage probability) of the communication system is effectively improved.

INDEX TERMS Intelligent transportation system (ITS), traffic estimation, integrated sensing and communication (ISAC), communication signals of opportunity, Jensen-Shannon (JS) divergence, leastsquares estimation (LSE), proactive mmWave beam allocation.

I. INTRODUCTION

Road traffic monitoring plays an important role in traffic management within the Intelligent Transportation System (ITS) [1], [2]. Metrics related to road traffic monitoring include **traffic density** (defined as number of vehicles per mile) and **traffic flow average speed**. These metrics can provide valuable insights for proactive traffic management, optimizing road construction scheduling, and facilitating prompt emergency responses [3]. Moreover, they have positive impacts on the society and environment [4]. For instance, real-time traffic density and flow speed information could be employed to provide a real-time route planning service to guide vehicles to avoid congested roads, thus reducing driving time, toxic gas emissions, and air pollution [5].

Several traffic monitoring techniques have been designed and developed over time. Traditional methods primarily rely on a large number of detectors, such as cameras, ultrasonic [7]. Such kinds of systems are accurate but exhibit some

The associate editor coordinating the review of this manuscript and approving it for publication was Adao Silva.

detectors, induction loop detectors, and radar sensors [6], shortcomings. Sometimes their detection performance is affected by the environment and bad weather conditions (e.g., fog, rain, etc.). In addition, these detection/estimation systems are typically complex and require fixed wired infrastructure for installation, which limits coverage of areas and leads to significant deployment time and costs, especially as the metropolis road networks grow rapidly [8]. Therefore, from both application and research perspectives, it is necessary to explore alternative techniques for traffic monitoring, such as radio-based approaches.

Numerous studies have explored traffic monitoring through vehicle-to-vehicle (V2V), vehicle-to-infrastructure (V2I), or vehicle-to-everything (V2X) communication methods [9], [10], [11]. These systems rely on connected vehicle technology to periodically exchange cooperative awareness messages to share information about traffic conditions. However, these systems encounter various challenges, such as short-range, large channel access delay, and huge capital investment. Moreover, as the use of connected vehicles becomes widespread, radio resource allocation becomes a major challenge. Additionally, these systems are vulnerable to security breaches due to the broadcast and unencrypted nature of wireless communications [12]. Therefore, there is a pressing need for cost-effective and scalable radio-based traffic sensing methods.

Over the past few years, ISAC has been emerging as a key enabler for future wireless systems to support many new applications [13], [14], [15], [16]. ISAC refers to a design paradigm and enabling technologies, in which sensing and communication systems are integrated to efficiently utilize congested resources [13] by sharing infrastructure and spectrum. The integration of functions not only reduces the overall cost but also leads to higher service quality due to the synergy between communication and sensing. Indeed,communication-assistedsensingandsensing-assisted communication can be achieved synergically in a single ISAC setup [16], [17], [18]. These features open up new possibilities, including radio-based road traffic monitoring for efficient and enhanced road traffic management within the ITS. One aspect of ISAC is the reuse of communication waveforms for sensing purposes. For instance, noncollaborative OFDM signals from illuminators of opportunity (IoO) can provide an efficient and effective solution to localize, detect, or track targets. The traffic sensing outcomes not only contribute to the transportation system but also can assist the communication system in allocating its resources proactively and effectively.

Several research works have developed passive radar sensing techniques by utilizing the signals transmitted from different kinds of IoOs to detect and localize targets. In [19], [20], different schemes were proposed for multitarget localization and speed estimation using OFDM signals from IoOs. In [21], the authors introduced a technique for target counting using OFDM signals. In [22], OFDM signals from a non-collaborative digital video broadcastingterrestrial (DVB-T) transmitter were used to detect moving targets. Also, some researchers developed a road traffic monitoring system to monitor density and speed using GSM-based transmitters [23]. Although the aforementioned systems somehow outperform the traditional traffic monitoring systems in terms of cost and effectiveness, they impose several challenges that need to be addressed. One major concern is that these systems can only detect a few targets [19], [20], [21], [22], [23], preventing them from estimating the traffic density of massive vehicles on a road section. Moreover, the idea of searching over the whole range-Doppler space to estimate the ranges and velocities of the targets requires both large signal bandwidth (for range-resolution [24]) and high power, and also incurs high computational complexity. On the other hand, pure datadriven traffic estimation techniques (e.g., machine learning) provide no insight into the physical mechanisms, are less traceable [25], and often require very large datasets [26].

In this paper, we consider an ISAC scheme in the fifthgeneration (5G) infrastructure to perform traffic monitoring using 6-GHz band signals of opportunity and incorporate proactive mmWave beam allocation aided by traffic sensing for vehicular users demanding high data rate services. Assume the system is capable of multi-beam forming and sweeping, possibly in a cloud-radio-access network (CRAN) [25], which enables centralized processing for joint communication and sensing. With such a configuration, multiple base stations (BSs) can perform (either communication or sensing) cooperatively. Having information about the traffic flow speed efficiently aids in route planning, guiding vehicles to the fastest routes [27], [28]. The traffic monitoring (sensing) results can be used as the prior knowledge to enhance communication functionality [29] in addition to its assistant role in traffic management. Specifically, the vehicle density information can guide proactive allocation of radio resources.

Major contributions of this paper are summarized as follows:

- We propose an efficient and cost-effective traffic density estimation technique that combines model-based and data-driven approaches. The technique relies on JensenShannon (JS)-divergence for classification and leastsquares estimation (LSE) for interpolation, requiring less labeling and training efforts compared to typical artificial intelligence (AI)-based techniques like neural networks.
- A traffic flow average speed estimation method using level crossing rate (LCR) is introduced to offer more information about the traffic flow without requiring additional measurement. This method is extended from

the original LCR-based technique that handles one or very few number of targets.

- We present a traffic-density-aware proactive beam allocation method for vehicular users demanding high data rate services in the area of interest, while minimizing the number of idle mmWave beams given an acceptable service outage.

TABLE 1. Major notations.

Notation	Description
N_s	Number of OFDM symbols
N_c	Number of OFDM subcarriers
N_v	Number of vehicles
σ_v	Radar cross section (RCS) of a vehicle
ξ_v	Whole-path attenuation factor due to propagation losses and RCS (σ_v) of a target
s_v	Vehicles average speed
N_l	Number of clutter objects
σ_l	Radar cross section (RCS) of a clutter object
ξ_l	Whole-path attenuation factor due to propagation losses and RCS (σ_l) of a clutter object
Δf	Subcarrier spacing
$Q(x)$	Probability density function (PDF) of a modeled template
M	Number of modeled PDF templates
$P(x)$	PDF of a testing signal
$p(N_v)$	Distribution of N_v vehicles
N^{α}_{LCR}	Cross number per second when signal envelope down-crosses a certain threshold A_{th}, or the "level crossing rate" (LCR)
ρ	Ratio of the threshold level A_{th} to the root mean square level of the envelope of received signal
$q(\epsilon\|N_v)$	Conditional distribution of estimation error ϵ
$\mathcal{E}_{Abs}$	Absolute mean square error
$\mathcal{E}_{Rel}$	Relative mean square error
N_B	Number of fixed beams
N_{max}	Maximum number of proactive beams provided by base station
N_{alo}	Number of allocated beams (proactive beam allocation)
P_{out}	Outage probability of fixed beam allocation
$\mathcal{P}_{out}$	Outage probability of proactive beam allocation
L	Mean number of idle beams (fixed beam allocation)
$\mathcal{L}$	Mean number of idle beams (proactive beam allocation)
$\mathcal{N}$	Number of training samples.
$\mathcal{M}$	Number of training classes.

- Comprehensive assessment and comparison are made based on simulations and analysis. In particular, two AI-based techniques, namely artificial neural networks (ANN) and K-means clustering, are considered as benchmarks in assessing the proposed traffic density estimation.

Generally speaking, our results suggest that the proposed scheme can efficiently estimate traffic density without requiring complex processing or extensive sets of measurement data. When compared to existing radio-based traffic estimation schemes, our method can handle a large number of targets by reusing communication waveforms, without the necessity of complex algorithms. It is worth noting that classification based on supervised learning usually uses a relatively large training dataset to teach/tune a classifier (models) to yield the desired output, while our pre-designed JS-divergence-based classifier is much more efficient. This is because it does not have many parameters to tune, and only needs to estimate a probability density function (PDF) of the received signal, without requiring a significantly large training data set.

Major notations used in the coming sections are given in Table 1. The rest of this paper is organized as follows. Section II presents related work. The system model is presented in Section III. The proposed schemes are described in Section IV. Quantitative assessment and comparison results are discussed in Section V, followed by conclusions in Section VI.

II. RELATED WORK

This section presents an overview of related research works that consider traffic density and flow speed estimation.

A. TRAFFIC DENSITY ESTIMATION

Extensive research on traffic density estimation systems has been conducted, and they can be categorized into four groups: *1)* ground-sensor-based, *2)* aerial-sensor-based, *3)* connected-vehicle-based, and *4)* data-driven approach.

1) GROUND-SENSOR-BASED SYSTEMS

Such systems commonly employ a large number of wireless sensors to collect road network information accurately [1], [30], [31], [32]. These sensors can be installed in various ways, either on the road surface or on the side of the road. Typical road surface sensors include inductive loops, magnetic detectors, and other weigh-in-motion devices. A notable example is the freeway performance measurement system (PeMS), which is employed by the California department of transportation (Caltrans). PeMS relies on real-time measurement data [33] gathered from inductive loops. The primary drawback of road surface sensors is the installation cost including sensors and supporting infrastructure, as these sensors are typically installed beneath the road surface. Furthermore, the cost of such a system increases if more lanes or new road sections need to be monitored. Other types of sensors installed on the sides of the road include cameras, microwave radars, and passive infrared sensors. While these sensors find widespread use, it is important to point out that their deployment and maintenance costs tend to be relatively high, and their performance can be susceptible to adverse weather conditions, as discussed in [32].

2) AERIAL-SENSOR-BASED SYSTEMS

These systems typically utilize unmanned aerial vehicles (UAVs) for road traffic monitoring [34]. Cameras mounted on UAVs perform traffic detection, making these systems costeffective due to their mobility and large geographic coverage. Consequently, they are well-suitable for fast data collection, but require complex post-processing algorithms to analyze images and video frames for traffic detection, as proposed in [6] and [35].

3) CONNECTED-VEHICLE-BASED SYSTEMS

These systems are usually in the vehicular ad-hoc network (VANET) framework, where vehicles and traffic infrastructure periodically exchange data through V2V, V2I, or V2X communication links. For instance, in [8], the authors proposed a reliable method for estimating traffic density by combining vehicle spacing information collected from a vehicular network and calculating the average spacing between vehicles in a specific area. While this technique offers good estimation accuracy, its implementation requires a substantial deployment of roadside units (RSUs), resulting inhighcosts.Certainly,thewidespreadadoptionofconnected vehicle technology can result in resource congestion. Also, these systems are vulnerable to security and privacy breaches due to the use of broadcast messages for exchanging information about traffic conditions.

4) DATA-DRIVEN APPROACH

In general, the implementation of the estimation methods mentioned above often incurs substantial installation efforts and high communication costs. Recent advances in wireless technology have introduced data-driven sensing techniques for traffic monitoring. Tulay and Koksal [36] proposed a passive traffic sensing scheme using dedicated shortrange communications signals transmitted from an RSU, where ''passive'' refers to making use of radio signals designated for other purposes. The scheme employs radio signal fingerprinting and machine learning for traffic density estimation. Furthermore, in their subsequent work [37], they introduced a traffic density estimation approach based on channel state information derived from signals transmitted by a transmitter on the RSU or a vehicle. This method also relies on machine learning and incorporates classification and regression algorithms to estimate the number of vehicles. However, the schemes presented in [36] and [37] can suffer from outages due to environmental changes and require a large dataset for accurate classification.

B. TRAFFIC FLOW SPEED ESTIMATION

Flow speed estimation can be divided into three categories: *1)* future flow speed estimation (actually, prediction), *2)* dedicated estimation, and *3)* wireless-signal-based estimation.

1) FUTURE FLOW SPEED ESTIMATION

These systems predict traffic flow for either a short or long period in the future. They rely on various time series models, such as historic average models [38], Bayesian network models [39], hidden Markov model [40], or the auto-regressive integrated moving average (ARMA) [41]. They operate under strict assumptions and conditions for prediction: there is clear awareness of the current traffic and complete historical speed measurements. Implementing such techniques can be challenging in the cases of limited measurements.

2) DEDICATED FLOW SPEED ESTIMATION

These systems offer traffic flow speed estimation with less required data compared to the prediction methods discussed above. Some of these approaches, as demonstrated in [42], leverage data collected from traffic sensors and employ the K-nearest neighbor method to infer real-time traffic speed. Other studies, such as [43], utilize videos collected from UAVs with an ensemble classifier (Haar cascade & convolutional neural network). Moreover, the scheme in [4], utilizes crowdsourcing vehicles that provide their real-time GPS records for speed estimation over a large region, and theyemployagraphconvolutionalgenerativeautoencoderfor real-time speed estimation. Although these methods provide accurate estimation, they either require complex and highcost system implementation [42], are negatively affected by bad weather conditions [43], or rely on connected vehicle technology [4].

3) WIRELESS-SIGNAL-BASED ESTIMATION

There are some works that explore the use of wireless signals for estimating the speed of a single mobile (vehicular) user, which could potentially be adapted for speed estimation for multiple mobile users. In [44], the authors presented an online algorithm for user equipment (UE) speed estimation in long term evolution-advanced (LTE-A) networks, using time-based spectrum spreading method (TSSM). The proposed method utilizes uplink LTE sounding reference signal (SRS) measurements conducted at the LTE base station. Specifically, the TSSM is employed as a metric for speed dependent time variations of the shadowing in the SRS measurements. A reference curve or lookup table (LUT, database) with respect to the shadowing decorrelation distance is created in advance. The computed values of the metric are then compared with the reference to determine a speed estimate. While this approach demonstrates good accuracy, it necessitates a huge database to attain the reported level of precision.

III. SYSTEM MODEL

A. SYSTEM ARCHITECTURE

We consider a system setup illustrated in Fig. 1 with two BSs and a number of vehicles on a multi-lane road section between the two BSs. The system supports dualband communication at mmWave band (e.g., 28 GHz, for bandwidth intensive services) and frequency division duplex (FDD) mid-band 5G (e.g., 6 GHz band). At the same time, the lower frequency band is used for traffic sensing in a fashion of bistatic radar using the communication signals of opportunity. The system performs dual-band communication and traffic sensing simultaneously. In the sensing mode, one BS (the left one in Fig. 1) serves as the IoO transmitting OFDM signals with radio beamwidth angle 30° (equivalent to a coverage of one mile of the road section), and another BS equipped with a dedicated receiver captures the signals reflected from vehicles. We assume the sensing receiver is able to significantly reduce the impact of the directpath component (from the transmitter to the receiver) using some techniques such as directional antenna, antenna array with nulling, or cancellation algorithm. Of course, more BSs can be employed, and the effectively illuminated area depends on how the system is geographically deployed and the beamwidths of the transmit and receive antennas. For mmWave communication, the mmWave transceivers can be mounted on one or both BSs. The traffic estimation results can be used for resource allocation tasks, such as downlink mmWave beam allocation (assuming one beam per vehicular user on the serviced road section). In addition, we assume certain system features, such as mmWave beamforming and beam sweeping, are available.

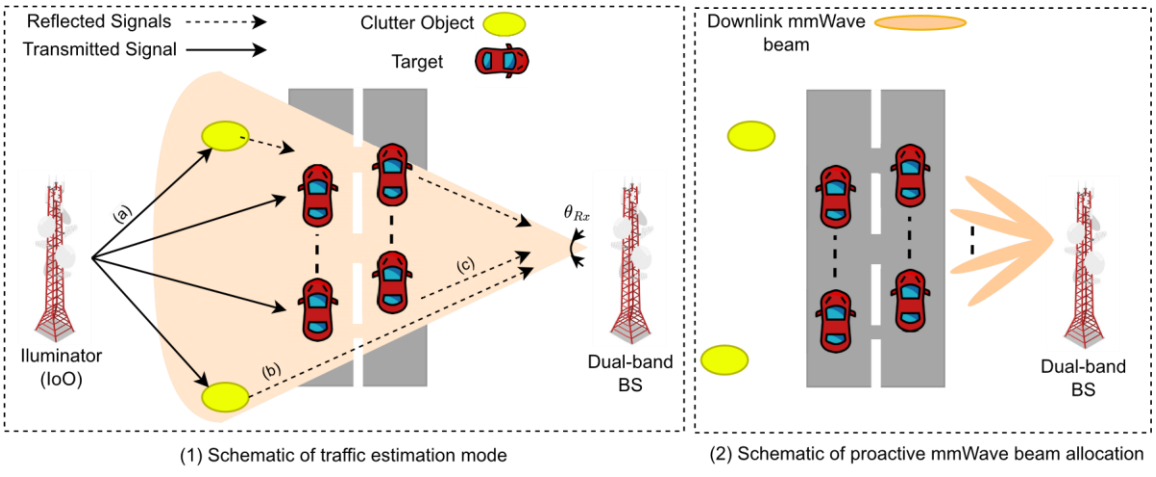

(a) IoO transmits a mid-band 5G signal. **(b)** Signals reflected from clutter objects. **(c)** Signals reflected from targets.

FIGURE 1. System setup of the proposed schemes considering a multi-lane scenario with clutter objects.

B. SIGNAL MODEL

Consider a transmitted OFDM signal consists of N_s OFDM symbols and N_c subcarriers. Such a signal at sample time t can be represented in baseband as follows:

$$x(t) = \sum_{m=0}^{N_s-1} \sum_{\kappa=0}^{N_c-1} X_{\kappa,m}\, e^{-j2\pi\kappa\Delta f (t-mT_s)} \cdot p g(t)\,, \quad (1)$$

where t is a time index, $X_{\kappa,m}$ is the communication data symbol modulated on the κth subcarrier and mth OFDM transmit symbol, where $\kappa = 0,1,\ldots,N_c-1$, and $m = 0,1,\ldots,N_s-1$, Δf is the subcarrier spacing between OFDM symbols, T_s is the length of an OFDM symbol, $g(t)$ is the impulse response of the raised cosine shaping filter [24].

Then, the transmitted passband OFDM signal can be expressed as:

$$\tilde{x}(t) = \mathcal{R}e\{x(t)\, e^{j2\pi f_c t}\}\,, \quad (2)$$

where f_c is the carrier frequency.

Assume the number of vehicles is N_v in the illuminated road section, where all vehicles can be considered as targets. Each target has a radar cross section (RCS) σ_v and an average speed s_v mph, $v = 0,\cdots,N_v-1$. In addition, there are N_l clutter objects that are not of interest, each of which has an RCS of σ_l, $l = 0,\cdots,N_l-1$. The transmitted signal is reflected from both vehicles and clutter objects, leading to the radio frequency (RF) passband received signal:

$$y(t) = \sum_{v=0}^{N_v-1} \sum_{m=0}^{N_s-1} \sum_{\kappa=0}^{N_c-1} \xi_v X_{\kappa,m}\, e^{j2\pi f_c(t-\tau_v)} \cdot e^{-j2\pi\kappa\Delta f (t-mT_s-\tau_v)} + \sum_{l=0}^{N_l-1} \sum_{m=0}^{N_s-1} \sum_{\kappa=0}^{N_c-1} \xi_l X_{\kappa,m}\, e^{j2\pi f_c(t-\tau_l)} \cdot e^{-j2\pi\kappa\Delta f (t-mT_s-\tau_l)} + n(t)\,, \quad (3)$$

where ξ_v and ξ_l represent the whole-path attenuation factors accounting for the propagation losses and RCSs (σ_v's and σ_l's) of the targets and clutter objects, respectively; τ_v and τ_l are the propagation delays corresponding to the targets and clutter objects, respectively; and $n(t)$ is the additive band limited Gaussian noise. (3) will be used to form a sensing channel in the simulation, where the propagation model for each path takes into account the total path loss and RCS, inthesamewayasusedinray-tracing-basedsimulations[36], [37]. Strictly speaking, ξ_v, ξ_l, τ_v and τ_l are time-varying random variables depending on the RCS and location of a vehicle. Because the received signal is a superposition of many random components, (3) is comparable to a fading channel model with many propagation paths, such as the Jakes and Cox model [45]. Indeed, observed from our simulation results, the received signal $y(t)$ does exhibit some fading behavior.

IV. PROPOSED SOLUTION AND ANALYSIS

In this section, we present our road traffic density and flow speed estimation schemes followed by the proactive beam allocation.

A. ROAD TRAFFIC DENSITY ESTIMATION

Different from traditional data-driven approaches, we do not use the received data directly to infer traffic density. Instead, aiming at the use of a smaller dataset and low computation complexity, we consider a hybrid approach involving both model-based and data-driven methods along with JS-divergence [46] used as an intermediate variable, where the JS-divergence is a distance measure between two probability density distributions, hence providing a way to compare the statistical characteristics. Two density

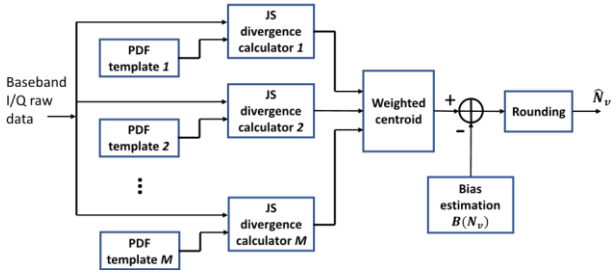

FIGURE 2. Architecture of proposed weighted-centroid-based traffic density estimator.

estimators, the weighted-centroid estimator and the optimal estimator, are proposed in this paper. The weighted-centroid density estimation is performed in four steps: 1) forming probability density function (PDF) templates of training classes based on the amplitude of the raw data received previously, 2) calculating current PDF based on just-received data (testing class) that corresponds to an unknown density to be estimated, 3) computing JS-divergence between the PDF templates of the training classes and current PDF of the testing class, and 4) estimating density based on weighted-centroid technique along with bias correction, using JS-divergence values as the weights. Fig. 2 shows a conceptual architecture of the proposed weighted-centroidbased traffic density estimator with $M(>1)$ parallel branches corresponding to the predefined M density levels. The optimal estimator contains four steps as well. The first three steps are similar to the weighted-centroid estimator, but the fourth step is to perform LSE utilizing the obtained JS-divergence values.

The proposed traffic density estimators do require labeled datasets. It is possible to obtain them by conducting a non-coordinated experiment without interrupting a normal transportation system. In the non-coordinated experiment, two raw data time series, i.e., the baseband I/Q sample streams and the vehicle-count sample stream, are generated and stored simultaneously over a sufficiently long time. Each vehicle count sample can be obtained based on an image snapshot of the road section, and it serves as the label of a segment of data samples. Then, the data sections with labels that fall in the required bins corresponding to the predefined density levels or classes (specific values of N_v) are selected as the templates for PDF estimation. Practical data collection and labeling are out scope of this paper.

In the first step, corresponding to M predefined training density classes, experiments are conducted to generate a dataset of M measurements $\{y_j[n], n = 1,2,3,\cdots, N \text{ and } j = 1,2,3,\cdots, M\}$, for training purposes. Here, N represents the number of data points for each class. We calculate the PDF templates using Kernel density estimation (KDE) [47]. N bins are employed in KDE, and the PDF estimated formula is as follows:

$$Q_j(x) = \frac{1}{Nh} \sum_{n=1}^{N} K\left(\frac{x - |y_j[n]|}{h}\right), \quad (4)$$

where K is a non-negative kernel function (e.g., normal) and h is a smoothing factor.(4)is used to generate M PDFtemplates of the training classes: $Q_1(x), Q_2(x), Q_3(x), \ldots, Q_M(x)$. Similarly, with measurement data $\{y[n], n = 1,2,3,\cdots, N\}$, wecanobtainameasuredPDF$P(x)$ofatestingclassinstep2. This testing class corresponds to data from an unknown number of vehicles.

Note that the JS-divergence is a smoothed version of the KL-divergence, and it is preferred since it is bounded $0 \le JS(\,) \le 1$ no matter what density N_v is, and symmetric so that the distance is independent of the order of the two PDFs under test.

In the third step, the JS-divergence between $P(x)$ and $Q_j(x)$ is calculated as follows:

$$JS\,P(x)||Q_j(x) = \frac{1}{2}KL\,P(x)||G_j(x)$$

where $G_j(x) = (1/2)\,P(x) + Q_j(x)$, and $KL(\quad)$ is the Kullback-Leibler (KL) divergence given by

$$||\quad = \sum_x \quad P(x) + \frac{1}{2}KL\,Q_j(x)||G_j(x), \tag{5}$$

$$KL\,P(x)\,G_j(x) \quad P(x)\,log_2, \quad (6)_x \quad G_j(x)$$

$$KL\,Q_j(x)||G_j(x) = \sum_x \frac{Q_j(x)}{Q_j(x)}\,log_2. \quad (7)_x \quad G_j(x)$$

With M JS-divergence values obtained in the third step, two types of estimators are explained as follows.

1) WEIGHTED-CENTROID ESTIMATOR

The weighted-centroid-based traffic density estimate is given by

$$\hat{N}_v = \frac{\sum_{j=1}^{M} N_{v(j)} JS\,P(x)||Q_j(x)}{\sum_{j=1}^{M} JS\,P(x)||Q_j(x)} - \hat{B}(N_v), \tag{8}$$

where $N_{v(j)}$ is the actual number of vehicles associated with the jth PDF template, and $\hat{B}(N_v)$ is an estimate of the bias between the actual and estimated vehicle densities. Note that pure weighted-centroid technique with JS-divergences as its weights does not guarantee unbiased estimation. Indeed, the bias is not zero according to some test results, and both noise and clutter should have impacts on the bias. An error correction process can be used to improve the estimation if the error estimate $\hat{B}(N_v)$ is available. Practically, the bias for a given clutter condition can be calibrated based on a set of S measurements $\hat{N}_{v,s}$:

$$\hat{B}(N_v) = \frac{1}{S}\sum_{s=1}^{S}(\hat{N}_{v,s} - N_v). \tag{9}$$

2) OPTIMAL ESTIMATOR

Define vectors η, ζ, and ζ_j:

$$\eta = N_{(1)}, N_{(2)}, \cdots, N_{(M)}^T, \tag{10}$$

$$JS\,P(x)||Q_1(x)\;\zeta = \frac{JS\,P(x)||Q_1(x)}{\sum_{j=1}^{M} JS\,P(x)||Q_j(x)}, \quad \cdots, \frac{JS\,P(x)||Q_M(x)}{\sum_{j=1}^{M} JS\,P(x)||Q_j(x)}, \tag{11}$$

$$\zeta^i = \frac{JS\,Q_i(x)||Q_1(x)}{\sum_{j=1}^{M} JS\,Q_i(x)\,Q\,(x)}\|_j, \quad \cdots, \frac{JS\,Q_i(x)||Q_M(x)}{\sum_{j=1}^{M} JS\,Q_i(x)||Q_j(x)}, \quad i = 1,2,3,M. \tag{12}$$

where (12) can be obtained by replacing $P(x)$ in (11) with known PDF $Q_i(x)$, $i = 1,2,3,M$. Form a matrix that is a stack of M JS-divergence vectors:

$$Z = \begin{bmatrix} \zeta_{T_1} \\ \vdots \\ \zeta_{TM} \end{bmatrix}. \tag{13}$$

$M \times M$

Then, consider a linear model

$$N_v = \zeta^T \omega, \; N_v^{(i)} = \zeta_i^T \omega, \qquad i = 1,2,3,\cdots,M, \tag{14}$$

where ω is an unknown $M \times 1$ weighting vector to be determined. Of course, a specific value of ω cannot perfectly satisfy all individual equations; instead, we need to find a weighting vector ω^* that is optimal overall. Note that $N_v^{(i)} = \zeta_i^T \omega$, $i = 1,2,3,\cdots,M$, in (14) can be rewritten in a compact form:

$$Z\omega = \eta, \tag{15}$$

which leads to the LSE solution:

$$\omega_* = ZZ^T{}^{-1} Z\eta, \tag{16}$$

and the optimal estimate is given by:

$$\hat{N_v} = \zeta^T \omega_*. \tag{17}$$

Note that only a limited number of templates $Q_j(x)$ are employed for training, but this does not prevent the estimator from handling a wide range of density levels.

B. TRAFFIC FLOW AVERAGE SPEED ESTIMATION

For the purpose of traffic management, we care about the traffic flow speed as a whole, instead of individual vehicle speed. Some existing work based on level crossing rate (LCR) [48] can be borrowed and extended for this purpose. The LCR of the envelope of post-processed received signal $y(t)$ is defined as the number of cross counts per second, where each count corresponds to an event that the envelope level down-crosses a certain threshold A_{th}. The LCR expression in Rayleigh fading channels has been derived in [49] and is expressed as:

$$\frac{N_{LCR}}{\rho} = \sqrt{2\pi}\,\rho\, e^{-\rho^2} \frac{s_v}{\lambda_c}, \tag{18}$$

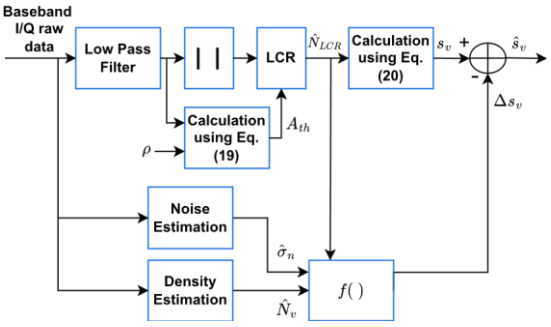

FIGURE 3. Traffic flow average speed estimator of multiple targets (vehicles).

where λ_c is the carrier wavelength and ρ is the ratio of the threshold level A_{th} to the root mean square level Y_{RMS} of the envelope of $y(t)$, which can be given as follows:

$$A_{th} = \rho\, Y_{RMS}. \tag{19}$$

For a single target, given the LCR value N_{LCR}^{ρ} from the received signal envelope, the estimated vehicle speed s_v can be obtained as:

$$s_v = \frac{e\,\lambda_c}{\sqrt{2\pi}} N_{LCR}^{\rho}. \tag{20}$$

Note that the value of ρ is used to control the threshold level at which the signal crosses. In many cases, $\rho = 1$ is chosen, representing a straightforward and common scenario where the signal level crosses a fixed threshold.

Inspired by what is described above, we consider a traffic flow speed estimator as illustrated in Fig. 3, where the low pass filter is to reduce the noise impact. The key idea is to correct the errors made by the pure LCR-based speed estimator originally designed for the single-vehicle case. As validated by simulation, the error can be regarded as a function $1s_v = f(\sigma_n, N_v, N_{LCR})$. Practically, $1s_v = f(\sigma_n, N_v, N_{LCR})$ can be implemented as a lookup table (LUT) approximated using experiment.

C. PROACTIVE BEAM ALLOCATION

In this application, we make use of our proposed traffic density estimation scheme to enhance the QoS of vehicular user communication. Specifically, we propose a proactive beam allocation technique that enables the BS to allocate antenna modules and mmWave beams based on the estimated number of vehicles. With proactive beam allocation, beam resources can be assigned to required vehicular users quickly. For comparison, we also consider fixed reservation as a benchmark. Note that beam alignment is out of scope of this paper and it can be done based on the location information of each vehicle, which can be obtained with the use of available positioning technologies during the requests process.

Assume vehicular users request radio beams for data communication, and the service requests follow the Poisson arrival model [50]. Consider a Poisson process with a mean arrival rate $\lambda = \alpha \cdot \tau$, where α is the number of packets transmitted in the time interval τ, and $\lambda > 0$. Then, the success probability of the BS to serve the vehicles using N_B mmWave beams can be expressed as:

$$P_{suc}(N_B | N_v, \lambda) = \sum_{r \le N_B} \frac{(N_v\lambda)^r e^{-N_v\lambda}}{r!}, \tag{21}$$

where r is the number of requests per vehicle. Note that to achieve successful communication for the active vehicles, the beam assignment should satisfy the constraint $r \le N_B$. If the probability that r exceeds the number of beams N_B, this is known as the outage probability, which can be represented as:

$$P_{out}(N_B | N_v, \lambda) = \sum_{r > N_B} \frac{(N_v\lambda)^r e^{-N_v\lambda}}{r!}, \tag{22}$$

Two beam allocation schemes are considered in this paper. Let us start with the **fixed beam allocation scheme**. In this scenario, a fixed number of beams N_B is allocated to serve the vehicles, where N_B can be chosen based on historical traffic data and it should not exceed the maximum number of beams N_{max} that BS can support. The outage probability $\bar{P}_{out}$ can be expressed as:

$$\bar{P}_{out}(\lambda) = \sum_{N_v} p(N_v) P_{out}(N_B | N_v, \lambda), \quad (23)$$

and the mean number of idle (not used) beams $\bar{L}$ is given by:

$$\bar{L}(\lambda) = \sum_{N_v} p(N_v) \sum_{r \le N_B} \frac{(N_v\lambda)^r}{r!} e^{-N_v\lambda} \cdot (N_B - r). \quad (24)$$

Note that the fixed beam allocation scenario does not provide flexibility and imposes coverage problems when the number of vehicles is greater than the number of allocated beams. Therefore, we propose a proactive beam allocation, which alleviates the problems of the fixed beam allocation.

For the **proactive beam allocation**, we introduce a control function $a(N_v + \epsilon) = a(\hat{N}_v)$ that is a predefined offset function (or lookup table) for adjusting the reservation level as N_v changes, where $\epsilon = \hat{N}_v - N_v$ is the estimation error. Practically, there must be a ceiling N_{max} for resource availability. The number of allocated beams can be expressed as

$$N_{alo} = round\, min\, N_{max}, \hat{N}_v\lambda + a(\hat{N}_v) = round\, min\, N_{max}, (N_v + \epsilon)\lambda + a(N_v + \epsilon), \quad (25)$$

where $round(\,)$ is the round function. The corresponding conditional outage probability (conditioned on N_v and a) is as follows:

$$P_{out}(N_v, a, \lambda) = \sum_{\epsilon} q(\epsilon | N_v)\, P_{out}\, N_{alo} | N_v, \lambda, \quad (26)$$

where $q(\epsilon|N_v)$ is a conditional distribution of estimation errors, and $P_{out}\, N_{alo}|N_v,\lambda$ can be calculated using (22) but replacing N_B with N_{alo}. Then, we have the outage probability of the proactive scheme:

$$\bar{P}_{out}(a,\lambda) = \sum_{N_v} p(N_v)\, P_{out}(N_v, a, \lambda). \quad (27)$$

Another important parameter is the mean number of idle beams (conditioned on N_v and a) that can be expressed as:

$$L(N_v, a, \lambda) = \sum_{\epsilon} q(\epsilon | N_v) \sum_{r \le N_{alo}} \frac{(N_v\lambda)^r e^{-N_v\lambda}}{r!} \cdot (N_{alo} - r), \quad (28)$$

and, the mean number of idle beams is:

$$\bar{L}(a,\lambda) = \sum_{N_v} p(N_v)\, L(N_v, a, \lambda). \quad (29)$$

Finally, the optimal beam allocation is to find the optimal control function given by

$$a^*(\hat{N}_v, \lambda) = \underset{a}{\operatorname{argmin}} \bar{L}(a,\lambda) \quad \text{s.t. } P_{out}(a,\lambda) \le b \quad (30)$$

where b is a pre-selected threshold representing the maximum tolerance of outage probability. It needs to be pointed out that in practice $a^*(\hat{N}_v, \lambda)$ is not easily obtainable and may be replaced by a suboptimal function.

V. QUANTITATIVE ASSESSMENT AND COMPARISON

A. SIMULATION SETUP

In our simulations, we evaluate traffic density estimation, flow speed estimation, and proactive beam allocation performances, assuming a geometrical-based single-bounce channel model and known path loss. The IoO is located at (−700, −50) m and a receive BS located at (2500,40) m. In the sensing mode, the IoO and the receive BS beamwidths intersect to cover a road section of one mile length. We consider the transmitted signal as an OFDM signal with N_c = 1024 subcarriers and a mid-band carrier frequency f_c = 6.8 GHz. For pulse shaping, a root-raised-cosine filter with a roll-off factor of 0.25 is utilized.

At the sensing receiver side, assume the received signals are reflected from vehicles with RCSs σ_v following the uniform distribution U ∼ [1,11] based on the experiments reported in [51]. The vehicles' average speed is s_v = 60 mph, and the separation distance between vehicles is a random number between [10 − 20] m. Note that the distribution of the vehicles on the lanes follows a uniform distribution with consideration of the specified separation constraint. The received signal $y(t)$ is divided into chunks, each chunk includes N = 41374 I/Q samples mixed with noise such that the signal-to-noise ratio (SNR) is 2.7 dB. Four PDF templates for $N_v \in \{2,20,50,100\}$ are considered for density estimation, and they are formed based on synthetic datasets

generated using simulation. We call these density classes {2,20,50,100} used for training as **training classes**. In performance evaluation, we use testing datasets corresponding to some classes (e.g., 35) that may not belong to the training classes, and we call these classes **testing classes**. The same terminologies are used for speed estimation.

TABLE 2. Setting of major simulation parameters.

Parameter	Value	Parameter	Value
# of subcarriers N_c	1024	RCS σ_v	$\mathcal{U}\sim[1,11]$
ISAC f_c	6.8 GHz	mmWave f_c	28 GHz
Bandwidth	20 MHz	Vehicles sep. dist.	$10-20$ m
SNR	2.7 dB	Average speed s_v	60 mph
# of PDF templates M	4	# of iterations	20
# of Fix. beams N_B	17	# of Proac. beams N_{max}	30

For proactive beam allocation, the mmWave beams operate at f_c = 28 GHz. For the comparison purpose, two additional schemes, i.e., fixed reservation and unlimited reservation, are considered as benchmarks. A semi-analytical approach, a mix of Monte Carlo simulation and analysis, is adopted to generate the allocation performance results.

Simulations are implemented on MATLAB R2020a running on a Windows 10 PC with an Intel Core i7 processor operating at 3.6 GHz and 16 GB RAM. The major simulation parameters used in the system evaluation of this paper are summarized in Table 2.

B. ERROR PERFORMANCE OF PROPOSED TRAFFIC DENSITY ESTIMATION

We initially assess the performance of the weighted-centroidbased estimator, followed by the evaluation of the LSE method.

Single-lane, two-lane, and three-lane scenarios are tested using simulation, and it is found they lead to very similar statistics. Fig. 4 shows the estimated PDF of the received signals for different numbers of vehicles considering the twolane scenario, suggesting that the PDF is close to Gaussian and the standard deviation of the received signal increases as the number of vehicles increases. Similar behavior is observed in both single-lane and three-lane scenarios.

The four JS-divergence values for a ground true of 35 vehicles are given in Table 3. First of all, one can see that the divergence values at each column are very close at different number of lanes. In other words, the divergence values are somehow independent of the number of lanes. For the ground true of 35 vehicles, the weighted-centroid estimator leads to an estimate $\hat{N}_v = 37.8$ for single-lane scenario, $\hat{N}_v = 38$ for two-lane scenario, and $\hat{N}_v = 38.1$ for three-lane scenario, which are close to the true number $N_v = 35$. Following that, we study the effect of clutter on the PDF templates estimation and weighted-centroid traffic density estimator. For the PDF templates estimation, we found that adding clutter objects does affect the PDF templates estimation, especially when there is a small number of vehicles ($N_v = 2$), as shown in Fig. 4 (b). Specifically,

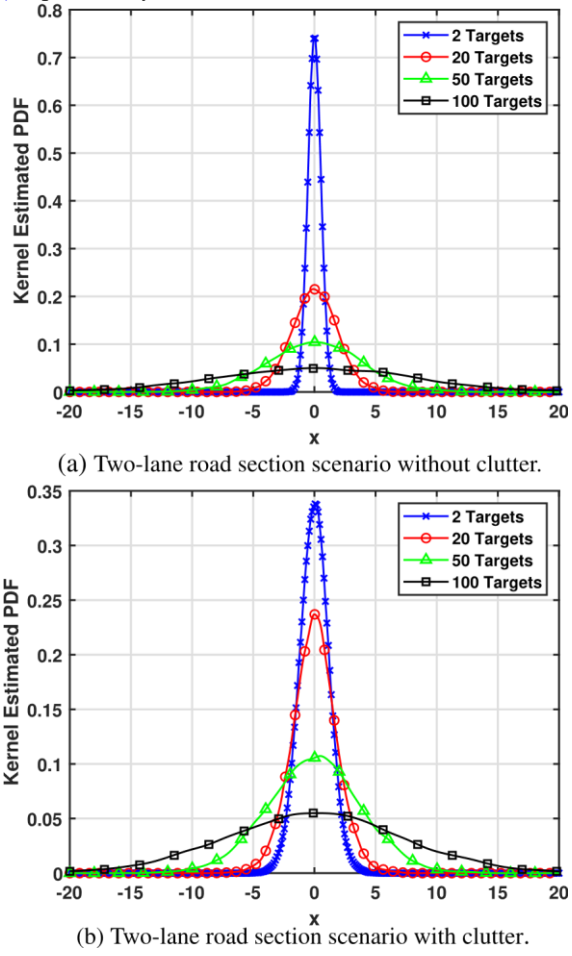

(a) Two-lane road section scenario without clutter.

(b) Two-lane road section scenario with clutter.

FIGURE 4. Estimated PDF of the received signal at different numbers of targets (two-lane scenario).

TABLE 3. JS-divergences (averaged over several trials) between the PDF templates of training classes and a PDF of testing class (35 vehicles) under no-clutter condition.

Number of vehicles	2	20	50	100
JS-div. (single-lane)	0.8018	0.3606	0.1895	0.5288
JS-div. (two-lane)	0.8192	0.3567	0.2102	0.5508
JS-div. (three-lane)	0.8130	0.3409	0.1878	0.5362

for the PDF template generated from ($N_v = 2$), its peak value was 0.75 with no clutter (see Fig. 4 (a)), and it was reduced to 0.35 when considering clutter (see Fig. 4 (b)). However, other PDF templates with a greater number of targets (N_v = 20,50,100) maintained the same values in both scenarios (clutter and no clutter). For traffic density estimation using the weighted-centroid method, the accuracy of the estimator does not change significantly; there is a slight offset of 15%.

Specifically, the estimated number of vehicles increased to 43 in the presence of clutter, compared to 38 with no clutter.

Furthermore, we test the optimal traffic density estimation using JS-divergence and LSE method. The estimator yields estimates of $\hat{N}_v = 35.6$, $\hat{N}_v = 35.7$, and $\hat{N}_v = 38.4$ for

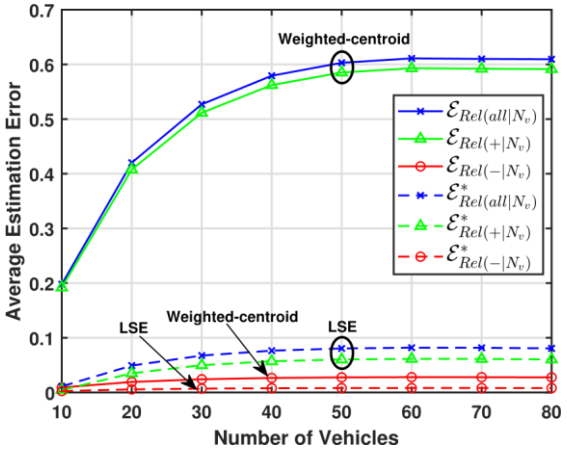

FIGURE 5. Average relative estimation errors over *Nv*.

the single-lane scenario, two-lane scenario with no clutter, and two-lane scenario with clutter, respectively. For threelane scenario, the estimates were $\hat{N}_v = 35.7$ without clutter and $\hat{N}_v = 38.8$ with clutter. Note that the clutter leads to a slight offset in the estimation similar to the weighted-centroid estimator.

Generally speaking, both estimators' performance remains consistent, whether considering a single-lane or two-lane scenario, and the estimation results in both scenarios closely align with each other. Additionally, the clutter does not degrade the performance of the estimators. Therefore, for performanceevaluation,weconsideratwo-lanescenariowith no clutter.

The estimation performance of both estimators is evaluated in mean square error (MSE) conditioned on the number of vehicles N_v. Specifically, the total absolute and relative MSEs conditioned on N_v can be calculated as follows:

$$\mathrm{E}_{Abs(\mathrm{S}|N_v)} = \sum_{\epsilon \in \mathrm{S}} \epsilon \, q(\epsilon|N_v), \tag{31}$$

$$\mathrm{E}_{Rel(\mathrm{S}|N_v)} = \frac{\mathrm{E}_{Abs(\mathrm{S}|N_v)}}{N_v}, \tag{32}$$

where error set S refers to ''all'' (i.e., all possible values for error ϵ), ''−ve'' error ($\epsilon < 0$), or ''+ve'' error ($\epsilon > 0$). If the PDF of N_v, $p(N_v)$, is known, then we have unconditional MSEs:

$$\bar{\mathrm{E}}_{Abs(\mathrm{S})} = \sum_{N_{v'}} p(N'_v) \mathcal{E}_{Abs(\mathcal{S}|Nv')}, \tag{33}$$

$$\bar{\mathrm{E}}_{Rel(\mathrm{S})} = \frac{\mathrm{E}_{Abs(\mathrm{S})}}{N_v}. \tag{34}$$

Note that we denote the optimal values of $\mathrm{E}_{Abs(\mathrm{S}|N_v)}$, $\mathrm{E}_{Rel}(\mathcal{S}|N_v)$, $\bar{\mathcal{E}}_{Abs(\mathcal{S})}$, $\bar{\mathcal{E}}_{Rel(\mathcal{S})}$ as $\mathcal{E}^*_{Abs(\mathcal{S}|N_v)}$, $\mathcal{E}^*_{Rel(\mathcal{S}|N_v)}$, $\bar{\mathcal{E}}^*_{Abs(\mathcal{S})}$, $\bar{\mathrm{E}}^*_{Rel(\mathrm{S})}$ which are corresponding to MSE obtained from the LSE method.

Fig. 5 shows the estimation errors conditioned on N_v for both weighted-centroid and the LSE method, where only four ($M = 4$) PDF templates are utilized for training, while the testing is conducted across $\{N_v = 10, 20, \cdots, 80\}$. The LSE

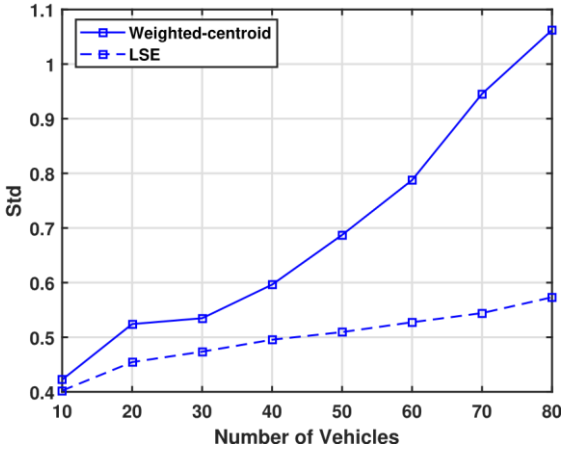

FIGURE 6. Standard deviation of estimation errors over *Nv*.

method exhibits lower average estimation error in all cases compared to the weighted-centroid. Additionally, in the LSE,
aslightbiasispresent,attributedtodifferencesinthestatistics between the training and testing datasets. However, it is clear that the weighted-centroid is a biased estimator, where the negative relative error $\bar{\mathrm{E}}_{Rel(-)}$ is smaller compared to the positive relative errors $\bar{\mathrm{E}}_{Rel(+)}$, suggesting that the estimator most likely outputs a number $\hat{N}_v$ greater than the true number N_v. This biased estimation tends to request slightly more mmWave beam allocation to reduce the outage probability. Note that the estimation bias $\mathrm{B}(N_v)$ is not zero and we may intentionally leave it as is for the weighted-centroid.

Fig. 6 illustrates the standard deviation (std) of estimation errors of both estimators, with the LSE method exhibiting a lower standard deviation in comparison to the weightedcentroid.

C. COMPARATIVE ASSESSMENT OF TRAFFIC DENSITY ESTIMATION

In this subsection, we conduct a thorough assessment by comparing our proposed scheme with two distinct AI-based

traffic density estimators, followed by a comparison with existing traffic density estimation schemes. Three estimation schemes are considered for comparison, and each scheme consists of two phases. Phase-1 is to measure distances between a set of predefined density levels (classes) and current density using some distance metric, while phase-2 estimates current density via some interpolation technique based on the distances obtained in phase-1.

In the AI-based approaches, the first method (see Fig. 7) combines artificial neural networks (ANN) and linear regression, while the second method employs K-means clustering in combination with linear regression. Note that linear regression is comparable to LSE.

1) C-1: SETUP OF MACHINE-LEARNING-BASED BENCHMARK DENSITY ESTIMATORS

For the ANN with linear regression, the ANN is used as a feature extractor before applying linear regression.

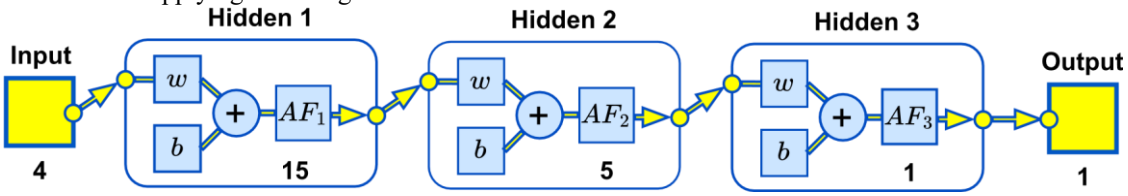

FIGURE 7. The structure of the implemented ANN used for comparison (*w* :weight, *b*:bias, and *AF* :activation function).

Specifically, in our study, the ANN is trained on four classes, each corresponding to the signals reflected from a known number of targets $N_v \in \{2,20,50,100\}$. This training allows the ANNto capturecomplex patternsand relationshipswithin the data. The output of the ANN serves as the input or features for the linear regression model. Then, linear regression is performed to fit (train) a linear model with the extracted feature data for estimating (inferring) an unknown number of cars (here $N_v = 35$ is used for testing) with a test dataset. Fig. 7 shows the structure of the implemented ANN. It includes 1 input layer, 3 hidden layers, and 1 output layer. 15, 5, and 1 neurons are contained at the first, second, and third hidden layers, respectively. The activation functions employed are as follows: AF_1 and AF_2 are both *Sigmoid* functions, while AF_3 is a linear regression function. T

For the K-means clustering-based density estimator, four (K = 4) clusters corresponding to the four levels of target densities $N_v \in \{2,20,50,100\}$ are established as references using the training dataset. After that, we generate a testing cluster using a test dataset with $N_v = 35$ targets, and calculate the distance between the test cluster and the four pre-trained reference clusters. Note that the distance between any two clusters is defined as the distance between their centroid points. Finally, we apply linear regression to find the estimated number of cars.

2) C-2: COMPLEXITY ANALYSIS

Asymptotic *Big* O complexity analysis of the three density estimators is provided in the following, assuming N is the number of training samples and M is the number of classes.

For the ANN model-based estimator, the time complexity is $O(N^2M^2)$, primarily due to the algorithm's training phase, which requires the most computational resources. The space complexity is determined by the amount of memory required for the algorithm to store the neural network parameters which is equal to $O(N^2M^2)$. Specifically, the algorithm needs to store neural network parameters, test data, and training data [52].

For estimation with K-means clustering, the time complexity of various operations is as follows: feature extraction takes O(NM), splitting the data into training and testing sets requires O(M), clustering the training data using Kmeans consumes O(NM*k*), feature extraction of the testing signal is O(M), calculating the average distance from the new signal to each cluster center takes O(*k*M). Then, the overall time complexity is O(NM*k*). The space complexity for K-means clustering is determined by several factors. The feature matrix and training data both contribute to a space complexity of O(NM). Additionally, the cluster centers introduce a space complexity of O(*k*M). When we combine these components, we obtain an overall space complexity of O(NM + *k*M) [53].

TABLE 4. Comparison between the proposed traffic density estimation scheme and two benchmark AI-based approaches we implemented for comparison purpose.

Metric	ANN	K-means Clustering	JS-div. with LSE
Size of Dataset	41347×200	41347×200	41347×4
$RMSD_{Rel}$	28.5%	12.3%	8.7%
Running Time (s)	17.84	12.77	1.03
Time Complexity	$\mathcal{O}(\mathcal{N}^2\mathcal{M}^2)$	$\mathcal{O}(\mathcal{N}\mathcal{M}k)$	$\mathcal{O}(\mathcal{N})$
Space Complexity	$\mathcal{O}(\mathcal{N}^2\mathcal{M}^2)$	$\mathcal{O}(\mathcal{N}\mathcal{M}+k\mathcal{M})$	$\mathcal{O}(\mathcal{N}\mathcal{M})$

In our proposed estimator, the time complexity is solely dependent on the number of training samples, which is equal to O(N). On the other hand, the space complexity is related to the memory needed for storing the signal samples corresponding to the PDF templates, resulting in a space complexity of O(NM).

3) C-3: SUMMARY OF COMPARISON

The comparison results between our scheme, ANN, and Kmeans clustering using the same raw data are summarized in Table 4. The evaluation is based on the following five key metrics: required size of dataset, relative mean square deviation ($RMSD_{Rel}$), running time, time complexity, and space (or computational) complexity. Notably, our scheme beats the two benchmark estimators with large margins in all considered metrics. This observation partially confirms that our pre-designed JS-divergence-based classifier has a superior structure with fewer parameters to tune, compared to the two supervised learning-based classifiers.

In addition, we qualitatively compare our scheme with several existing traffic density estimation schemes, as a quantitative comparison is not quite feasible. Table 5 highlights the major differences between our scheme and the traffic density estimation methods presented in [6], [9], [31], and [36]. As indicated in Table 5, the majority of existing schemes are considered as ''active'' estimation schemes, which introduce additional communication and computation overheads. Also, they rely on AI-based approaches for traffic density estimation, requiring large labeled datasets and involving complex algorithms.

TABLE 5. Comparison with existing traffic density estimation schemes.

[31]	Sensor-based	Active	Vision-based (fixed cameras) with AI	Large	×	√	Huge	High
[6]	Aerial-based	Active	Vision-based (UAV camera) with AI	Large	×	√	Huge	High
[9]	Radio-based	Active	V2I DSRC signals with AI	Large	√	×	Huge	High
[36]	Radio-based	Passive	V2I DSRC signals with AI	Large	√	×	Huge	High
Ours	Radio-based	Passive	IoO OFDM signals with JS-divergence & LSE	Large	√	√	Small	Low
	Category	Active/Passive	Methodology	# of Cars	Bad Weather	Dynamic Environment	Size of Dataset	Complexity

Note: The symbol (√) denotes a realized functionality and the symbol (×) denotes an unrealized functionality.

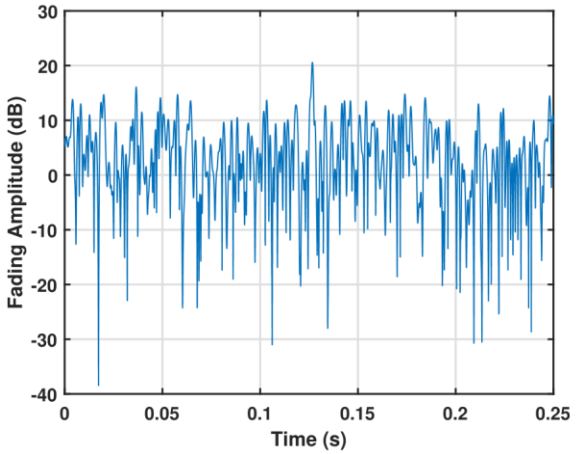

FIGURE 8. Fading amplitude for 20 vehicles moving at speed 60 MPH.

Although the scheme proposed in [36] is categorized as a passive traffic density estimation scheme, it still requires a relatively large training dataset to teach/tune the machine learning classifier to produce the desired estimation output.

In summary, our proposed scheme can effectively and efficiently estimate traffic density with a much smaller size of dataset. Moreover, it is promising to adapt to bad weather conditions and dynamic environments.

D. ASSESSMENT OF TRAFFIC FLOW AVERAGE SPEED ESTIMATION

Synthetic data is used to assess the proposed traffic flow speed estimation. Specifically, we measure the fading amplitude of signals reflected from vehicles moving at speeds $s_v = \{45, 60, 70\}$ mph over different density levels. Fig. 8 illustrates the fading amplitude of a signal received from 20 vehicles moving at a speed of 60 mph, and this result is utilized for calculating the LCR. Error function $1s_v = f(\sigma_n, N_v, N_{LCR})$ is implemented using a LUT based on the measurements (synthetic training data).

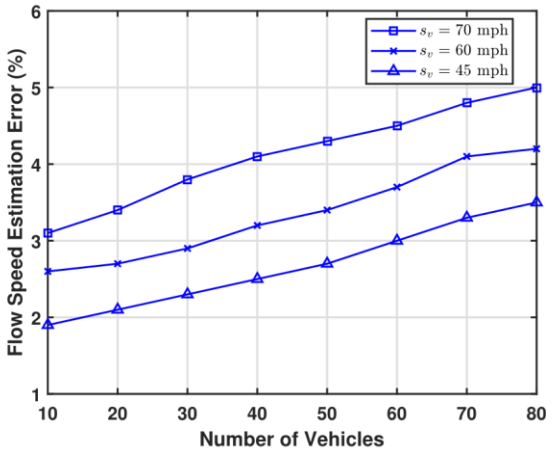

FIGURE 9. Average flow speeds estimation errors at different number of vehicles.

The accuracy of the estimator can be measured in absolute root mean square error deviation (RMSD):

$$RMSD = \sqrt{\frac{\sum_{t=1}^{T}(\hat{s}_{vt} - s_{vt})^2}{T}}, \quad (35)$$

T

where $\tilde{s}_{vt}$ is the speed estimation at iteration t, s_{vt} is the actual average speed, and T is the number of iterations.

The quality of the proposed traffic speed estimator is shown in Fig. 9, displaying the *RMSD* over diverse numbers of vehicles. One can see that the *RMSD* increases as the density and speed increase. This phenomenon seems to agree with our observation that moving speed and the number of vehicles contribute to the randomness of the fading signal.

E. ASSESSMENT OF BEAM ALLOCATION

For evaluating the beam allocation strategies, we consider five candidates as shown in Fig. 10, where (*i*) **simpleproactive with ceiling** and (*ii*) **optimal-proactive with ceiling** are two proposed practical strategies, while the rest are three reference candidates for comparison.

The proactive scheme includes an adjustable control function to proactively allocate the beams based on the current density estimate obtained using weighted-centroid or LSE methods. For the simple version, the control function

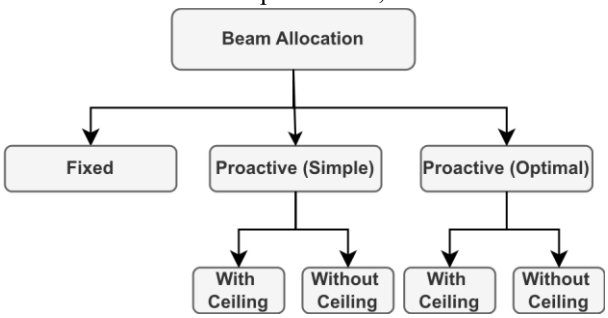

FIGURE 10. Beam allocation strategies considered for assessment (''Without Ceiling'' means $N_{max} \to \infty$).

$a(\hat{N}_v)$ is defined as

$$a(\hat{N}_v) = max0, round\ \gamma \cdot \lambda \cdot \hat{N}_v, \qquad (36)$$

where γ is a positive real constant (γ can be chosen in the simulation). For the optimal version, $a(\hat{N}_v)$ is computed using (30).

Fig. 11 (a), 11 (b), and 11 (c) show evaluation results of outage and beam waste, respectively, for three strategies of *fixed*, *simple-proactive with ceiling* and *simple-proactive withoutceiling*. The results are semi-analytically obtained for different numbers of vehicles N_v estimated using weightedcentroid or LSE methods, assuming a uniform distribution of $N_v \in [10,80]$. For the fixed-allocation benchmark scheme, $N_B = 17$ is selected. For simple proactive allocation, the number of allocated beams is equal to N_{alo} defined in (25) withthecontrolfunctiongivenby(36).Forthe''withceiling'' scenario, the ceiling values N_{max} are set to either 12, 20, or 30, while for the ''without ceiling'' scenario $N_{max} \to \infty$.

As expected and observed from Fig. 11 (a), the proactive schemes experience fewer outages compared to the fixed scheme, which improves the QoS accordingly. This improvement is attributed to the proactivity backed up by the real-time traffic density estimation. Note that the simpleproactive ''without ceiling'' achieves an outage probability lower bound close to zero ($P_{out} \approx 0$) at the cost of unlimited resource occupation ($N_{max} \to \infty$). However, in scenarios with extremely limited resources (e.g., the ceiling N_{max} set to a low value like 12), the proactive scheme may experience a higher outage compared to the fixed scheme. Moreover, it is evident that the outage probability for the beam allocation schemes over different numbers of vehicles estimated using LSE is lower compared to the weighted-centroid-based method. This is because the weighted-centroid is biased towards positive errors, resulting in a vehicle density estimate greater than the actual number, thereby requiring a larger number of beams.

On the other hand, the level of resource waste is evaluated using the mean number of idle beams ($\bar{L}$ and $\bar{L}$) as a metric. As shown in Fig. 11 (b) and 11 (c), the simple-proactive ''withoutceiling''exhibitsthehighestlevelofresourcewaste, with the level of resource waste increasing gradually as the numberofvehiclesrises.Thisbecausethecalculationof*Nalo*

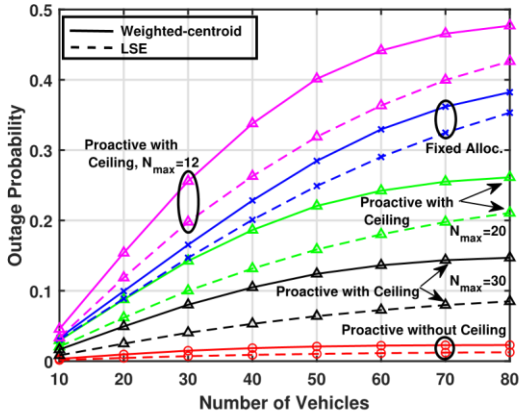

(a) Outage probability comparison of beam allocation strategies based on number of vehicles estimated using weighted-centroid and LSE.

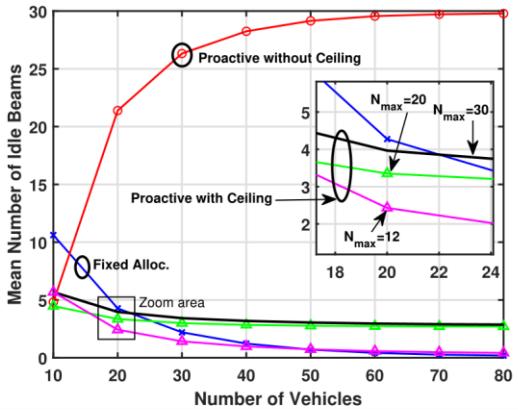

(b) Mean number of idle beams comparison obtained using weighted-centroid at different numbers of vehicles.

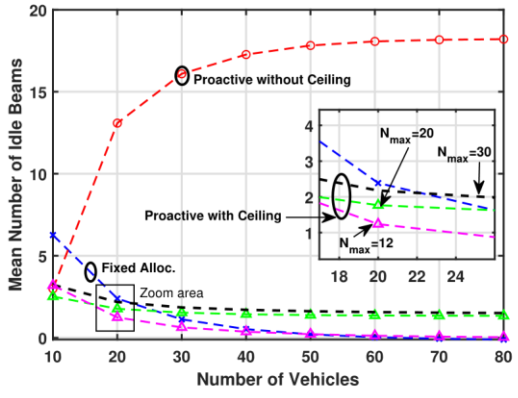

(c) Mean number of idle beams comparison obtained using weighted-centroid at different numbers of vehicles.

FIGURE 11. Evaluation of fixed, simple-proactive with ceiling, and simple-proactive without ceiling beam allocation strategies.

is primarily dependent on the term $(\hat{N}_v\lambda + a(\hat{N}_v))$ in (25), while it neglects the role of $min\ N_{max}, N_{ev}\lambda + a(N_{ev})$ due to theoretically unlimited resources available ($N_{max} \to \infty$). Specifically, when $N_v = 80$, this level of waste reaches approximately $\bar{L} \approx 30$ for the weighted-centroid and $\bar{L} \approx 18$ for the LSE. In the case of the simple-proactive

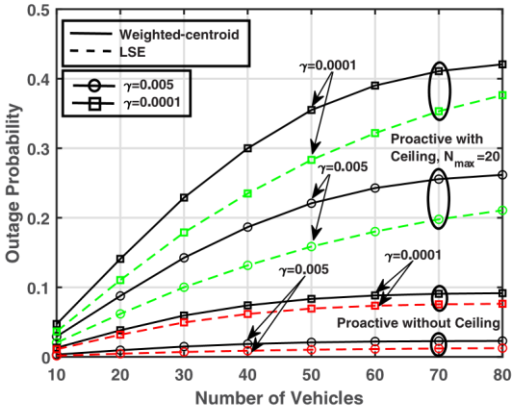

(a) Outage probability comparison of beam allocation strategies based on number of vehicles estimated at different γ's.

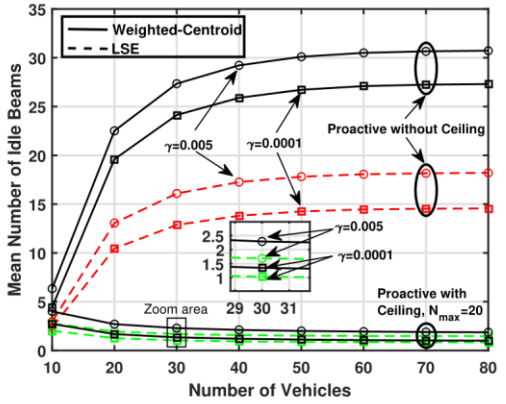

(b) Mean number of idle beams comparison over different numbers of vehicles and different γ's.

FIGURE 12. Evaluation of fixed, simple-proactive with ceiling, and simple-proactive without ceiling beam allocation strategies.

strategy ''with ceiling'', the level of resource waste varies less as the number of vehicles changes compared to the fixed strategy. This is due to the proactivity of our scheme, which can adapt the number of reserved beams based on the number of estimated vehicles. Interestingly, there is a turning point at $N_v = 20$ in Fig. 11 (b) and 11 (c), and the proactive scheme outperforms the fixed counterpart when $N_v < 20$; as N_v increases, the proactive scheme approximately maintains a small constant level of idleness. However, in scenarios with extremely limited resources ($N_{max} = 12$), the proactive scheme exhibits a lower level of idleness. Similar to the outage probability analysis, the LSE method exhibits a lower level of resource waste (see Fig. 11 (c)) compared to the weighted-centroid (see Fig. 11 (b)). This is because the weighted-centroid, with its positive bias, allocates a larger number of beams than needed. Note that the overall beam allocation performance is measured by both outage and idleness, and it can be stated that as the number of vehicles increases, the

simple-proactive ''with ceiling'' scheme performs significantly better than the fixed strategy at a minor penalty of $\bar{L} \approx 1.3$.

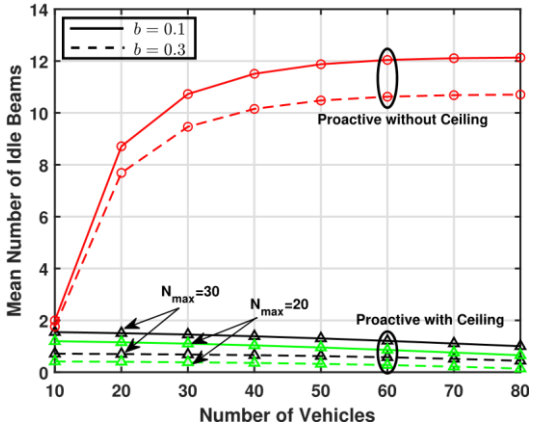

FIGURE 13. Mean number of idle beams comparison with optimal beam allocation at different numbers of vehicles estimated using LSE.

Next, we investigate the impact of the control parameter γ on the outage probability and the level of waste resource over different numbers of vehicles estimated using weightedcentroid and LSE methods. As shown in Fig. 12 (a), increasing the value γ leads to a decrease in the outage probability for both weight-centroid and LSE methods. On the other hand, as depicted in Fig. 12 (b), a reduction in γ values correlates with a decrease in the level of wasted resources.

The aforementioned (simple) proactive schemes can be further improved to reach the optimum by selecting the control function $a(\cdot)$ using (30), jointly considering the beam waste and outage. We emphasize our focus on the LSE method due to its superior estimation accuracy and the fact that it serves as an unbiased estimator. Fig. 13 illustrates the mean number of idle beams with optimal allocation based on (30) for both proactive beam allocation schemes (with ceiling and without ceiling). Generally, one can observe that the optimal-proactive beam allocation scheme exhibits a lower level of waste resource compared to the simple proactive schemes (see Fig. 11 (c)). Moreover, according to Fig. 13, the optimal beam allocation ''without ceiling'' under a given outage constraint $b = 0.1$ exhibits a larger number of idle beams ($\bar{L} \approx 14$) when compared to the scenario with ceilings ($\bar{L} \approx 0.8$). This behavior remains consistent when increasing the threshold b to 0.3. In conclusion, it's evident that for both the simple and optimal proactive strategies, scenarios ''without ceiling'' consistently exhibit a larger average number of idle beams, which increases gradually as the number of vehicles rises, due to the unlimited resources. This highlights the importance of the ceiling in effectively restricting $\bar{L}$.

VI. CONCLUSION AND FUTURE WORK

This paper presents an efficient and cost-effective traffic monitoring scheme to support ITS by leveraging the synergy between sensing and communication in an ISAC framework. The proposed scheme reuses the communication waveform for estimating both traffic density and speed, and simultaneously enhances the connectivity and QoS for vehicular users via proactively allocating mmWave beams aided by the traffic density estimation. The performance analysis and comparison show that the proposed traffic estimators require less training, are computationally efficient, and can yield accurate estimates at diverse vehicle density levels. The assessment results also suggest that proactive beam allocation is very promising due to its superiority over fixed beam allocation. As a matter of fact, the traffic sensing outcomes can benefit different resource allocation tasks. Also, the proposed mmWave beam allocation scheme can be directly used for channel allocation in lower frequency bands. Numerous related topics can be further explored in the future, such as combining beam sweeping techniques with beam allocation, considering more practical traffic scenarios, and further improving the estimators.

REFERENCES

[1] A. Thakur and R. Malekian, ''Fog computing for detecting vehicular congestion, an Internet of Vehicles based approach: A review,'' *IEEE Intell. Transp. Syst. Mag.*, vol. 11, no. 2, pp. 8–16, Summer 2019.

[2] Z. Liu, Y. Liu, Q. Meng, and Q. Cheng, ''A tailored machine learning approach for urban transport network flow estimation,'' *Transp. Res. C, Emerg. Technol.*, vol. 108, pp. 130–150, Nov. 2019.

[3] E. Hossain, G. Chow, V. C. M. Leung, R. D. McLeod, J. Mišić, V. W. S. Wong, and O. Yang, ''Vehicular telematics over heterogeneous wireless networks: A survey,'' *Comput. Commun.*, vol. 33, no. 7, pp. 775–793, May 2010.

[4] J. J. Q. Yu and J. Gu, ''Real-time traffic speed estimation with graph convolutional generative autoencoder,'' *IEEE Trans. Intell. Transp. Syst.*, vol. 20, no. 10, pp. 3940–3951, Oct. 2019.

[5] J. Zhang, F.-Y. Wang, K. Wang, W.-H. Lin, X. Xu, and C. Chen, ''Datadriven intelligent transportation systems: A survey,'' *IEEE Trans. Intell. Transp. Syst.*, vol. 12, no. 4, pp. 1624–1639, Dec. 2011.

[6] J. Zhu, K. Sun, S. Jia, Q. Li, X. Hou, W. Lin, B. Liu, and G. Qiu, ''Urban traffic density estimation based on ultrahigh-resolution UAV video and deep neural network,'' *IEEE J. Sel. Topics Appl. Earth Observ. Remote Sens.*, vol. 11, no. 12, pp. 4968–4981, Dec. 2018.

[7] I. Bisio, C. Garibotto, H. Haleem, F. Lavagetto, and A. Sciarrone, ''A systematic review of drone based road traffic monitoring system,'' *IEEE Access*, vol. 10, pp. 101537–101555, 2022.

[8] J. Wang, Y. Huang, Z. Feng, C. Jiang, H. Zhang, and V. C. M. Leung, ''Reliable traffic density estimation in vehicular network,'' *IEEE Trans. Veh. Technol.*, vol. 67, no. 7, pp. 6424–6437, Jul. 2018.

[9] S. M. Khan, K. C. Dey, and M. Chowdhury, ''Real-time traffic state estimation with connected vehicles,'' *IEEE Trans. Intell. Transp. Syst.*, vol. 18, no. 7, pp. 1687–1699, Jul. 2017.

[10] R. Bauza and J. Gozalvez, ''Traffic congestion detection in large-scale scenarios using vehicle-to-vehicle communications,'' *J. Netw. Comput. Appl.*, vol. 36, no. 5, pp. 1295–1307, Sep. 2013.

[11] A. M. de Souza, R. S. Yokoyama, L. C. Botega, R. I. Meneguette, and L. A. Villas, ''Scorpion: A solution using cooperative rerouting to prevent congestion and improve traffic condition,'' in *Proc. IEEE Int. Conf. Comput. Inf. Technol., Ubiquitous Comput. Commun., Dependable, Autonomic Secure Comput., Pervasive Intell. Comput.*, Oct. 2015, pp. 497–503.

[12] S. Gyawali, S. Xu, Y. Qian, and R. Q. Hu, ''Challenges and solutions for cellular based V2X communications,'' *IEEE Commun. Surveys Tuts.*, vol. 23, no. 1, pp. 222–255, 1st Quart., 2021.

[13] Y. Cui, F. Liu, X. Jing, and J. Mu, ''Integrating sensing and communications for ubiquitous IoT: Applications, trends, and challenges,'' *IEEE Netw.*, vol. 35, no. 5, pp. 158–167, Sep. 2021.

[14] A. Liu, Z. Huang, M. Li, Y. Wan, W. Li, T. X. Han, C. Liu, R. Du, D. K. P. Tan, J. Lu, Y. Shen, F. Colone, and K. Chetty, ''A survey on fundamental limits of integrated sensing and communication,'' *IEEE Commun. Surveys Tuts.*, vol. 24, no. 2, pp. 994–1034, 2nd Quart., 2022.

[15] M. M. Şahin, I. E. Gurol, E. Arslan, E. Basar, and H. Arslan, ''OFDMIM for joint communication and radar-sensing: A promising waveform for dual functionality,'' *Frontiers Commun. Netw.*, vol. 2, Aug. 2021, Art. no. 715944.

[16] J. Wang, N. Varshney, C. Gentile, S. Blandino, J. Chuang, and N. Golmie, ''Integrated sensing and communication: Enabling techniques, applications, tools and data sets, standardization, and future directions,'' *IEEE Internet Things J.*, vol. 9, no. 23, pp. 23416–23440, Dec. 2022.

[17] F. Liu, Y. Cui, C. Masouros, J. Xu, T. X. Han, Y. C. Eldar, and S. Buzzi, ''Integrated sensing and communications: Toward dual-functional wireless networks for 6G and beyond,'' *IEEE J. Sel. Areas Commun.*, vol. 40, no. 6, pp. 1728–1767, Jun. 2022.

[18] D. K. Pin Tan, J. He, Y. Li, A. Bayesteh, Y. Chen, P. Zhu, and W. Tong, ''Integrated sensing and communication in 6G: Motivations, use cases, requirements, challenges and future directions,'' in *Proc. 1st IEEE Int. Online Symp. Joint Commun. Sens. (JC&S)*, Feb. 2021, pp. 1–6.

[19] Y. Li, X. Wang, and Z. Ding, ''Multi-target position and velocity estimation using OFDM communication signals,'' *IEEE Trans. Commun.*, vol. 68, no. 2, pp. 1160–1174, Feb. 2020.

[20] U. K. Singh, V. Bhatia, and A. K. Mishra, ''Multiple target detection and estimation of range and Doppler for OFDM-RADAR system,'' in *Proc. 4th Int. Conf. Signal Process. Integr. Netw. (SPIN)*, Feb. 2017, pp. 27–32.

[21] S. Bartoletti, A. Conti, and M. Z. Win, ''Towards counting via passive radar using OFDM waveforms,'' in *Proc. IEEE Int. Conf. Commun. Workshops (ICC Workshops)*, May 2017, pp. 803–808.

[22] G. Gassier, G. Chabriel, J. Barrère, F. Briolle, and C. Jauffret, ''A unifying approach for disturbance cancellation and target detection in passive radar using OFDM,'' *IEEE Trans. Signal Process.*, vol. 64, no. 22, pp. 5959–5971, Nov. 2016.

[23] M. K. Baczyk, P. Samczynski, P. Krysik, and K. Kulpa, ''Traffic density monitoring using passive radars,'' *IEEE Aerosp. Electron. Syst. Mag.*, vol. 32, no. 2, pp. 14–21, Feb. 2017.

[24] Y. Liu, G. Liao, Y. Chen, J. Xu, and Y. Yin, ''Super-resolution range and velocity estimations with OFDM integrated radar and communications waveform,'' *IEEE Trans. Veh. Technol.*, vol. 69, no. 10, pp. 11659–11672, Oct. 2020.

[25] T. N. Guo, A. B. MacKenzie, and H. Li, ''Interferometry based integrated sensing and communications with imperfect synchronizations,'' in *Proc. IEEE Global Commun. Conf. (GLOBECOM)*, Dec. 2021, pp. 1–6.

[26] H. Salem, M. Quamar, A. Mansoor, M. Elrashidy, N. Saeed, and M. Masood, ''Data-driven integrated sensing and communication: Recent advances, challenges, and future prospects,'' 2023, *arXiv:2308.09090*.

[27] H. Hu, G. Li, Z. Bao, Y. Cui, and J. Feng, ''Crowdsourcing-based real-time urban traffic speed estimation: From trends to speeds,'' in *Proc. IEEE 32nd Int. Conf. Data Eng. (ICDE)*, May 2016, pp. 883–894.

[28] Y.-S. Jeong, Y.-J. Byon, M. M. Castro-Neto, and S. M. Easa, ''Supervised weighting-online learning algorithm for short-term traffic flow prediction,'' *IEEE Trans. Intell. Transp. Syst.*, vol. 14, no. 4, pp. 1700–1707, Dec. 2013.

[29] A. K. Gizzini, M. Chafii, A. Nimr, R. M. Shubair, and G. Fettweis, ''CNN aided weighted interpolation for channel estimation in vehicular communications,'' *IEEE Trans. Veh. Technol.*, vol. 70, no. 12, pp. 12796–12811, Dec. 2021.

[30] S. R. E. Datondji, Y. Dupuis, P. Subirats, and P. Vasseur, ''A survey of vision-based traffic monitoring of road intersections,'' *IEEE Trans. Intell. Transp. Syst.*, vol. 17, no. 10, pp. 2681–2698, Oct. 2016.

[31] T. Pamula, ''Road traffic conditions classification based on multilevel filtering of image content using convolutional neural networks,'' *IEEE Intell. Transp. Syst. Mag.*, vol. 10, no. 3, pp. 11–21, Fall. 2018.

[32] D. R. Middleton, R. Longmire, S. Turner, and D. Middleton, ''State of the art evaluation of traffic detection and monitoring systems. Volume 1, phases A & B: Design,'' Arizona Dept. Transp., Phoenix, AZ, USA, Tech. Rep., 2007.

[33] Georgia Dept. Transp. (2022). *Challenges of the Day to Day Operation of a Traffic Monitoring Program*. [Online]. Available: http://onlinepubs.trb.org/onlinepubs/conferences/2016/NATMEC/WiegandTannerPPT.pdf

[34] K. Kanistras, G. Martins, M. J. Rutherford, and K. P. Valavanis, ''A survey of unmanned aerial vehicles (UAVs) for traffic monitoring,'' in *Proc. Int. Conf. Unmanned Aircr. Syst. (ICUAS)*, May 2013, pp. 221–234.

[35] X. Zhao, D. Dawson, W. A. Sarasua, and S. T. Birchfield, ''Automated traffic surveillance system with aerial camera arrays imagery: Macroscopic data collection with vehicle tracking,'' *J. Comput. Civil Eng.*, vol. 31, no. 3, May 2017, Art. no. 04016072.

[36] H. B. Tulay and C. E. Koksal, ''Increasing situational awareness in vehicular networks: Passive traffic sensing based on machine learning,'' in *Proc. IEEE 91st Veh. Technol. Conf. (VTC-Spring)*, May 2020, pp. 1–7.

[37] H. B. Tulay and C. E. Koksal, ''Road state inference via channel state information,'' *IEEE Trans. Veh. Technol.*, vol. 72, no. 7, pp. 8329–8341, Jul. 2023.

[38] Z.-X. Huang, ''An analysis and discussion on short-term traffic flow forecasting,'' *Syst. Eng.*, Jan. 2003. [Online]. Available: https://api.semanticscholar.org/CorpusID:63899112

[39] X. Fei, C.-C. Lu, and K. Liu, ''A Bayesian dynamic linear model approach for real-time short-term freeway travel time prediction,'' *Transp. Res. C, Emerg. Technol.*, vol. 19, no. 6, pp. 1306–1318, Dec. 2011.

[40] B. Yang, C. Guo, and C. S. Jensen, ''Travel cost inference from sparse, spatio temporally correlated time series using Markov models,'' *Proc. VLDB Endowment*, vol. 6, no. 9, pp. 769–780, Jul. 2013.

[41] M. Lippi, M. Bertini, and P. Frasconi, ''Short-term traffic flow forecasting: An experimental comparison of time-series analysis and supervised learning,'' *IEEE Trans. Intell. Transp. Syst.*, vol. 14, no. 2, pp. 871–882, Jun. 2013.

[42] R. Zhong, G. Li, K.-L. Tan, L. Zhou, and Z. Gong, ''G-tree: An efficient and scalable index for spatial search on road networks,'' *IEEE Trans. Knowl. Data Eng.*, vol. 27, no. 8, pp. 2175–2189, Aug. 2015.

[43] R. Ke, Z. Li, J. Tang, Z. Pan, and Y. Wang, ''Real-time traffic flow parameter estimation from UAV video based on ensemble classifier and optical flow,'' *IEEE Trans. Intell. Transp. Syst.*, vol. 20, no. 1, pp. 54–64, Jan. 2019.

[44] M. Haddad, D. G. Herculea, C. S. Chen, E. Altman, and V. Capdevielle, ''Online mobile user speed estimation: Performance and tradeoff considerations,''in*Proc.14thIEEEAnnu.Consum.Commun.Netw.Conf.(CCNC)*, Jan. 2017, pp. 974–979.

[45] W. C. Jakes and D. C. Cox, *Microwave Mobile Communications*. Hoboken, NJ, USA: Wiley, 1994.

[46] B. Fuglede and F. Topsoe, ''Jensen–Shannon divergence and Hilbert space embedding,'' in *Proc. Int. Symp. Inf. Theory (ISIT)*, Jul. 2004, pp. 1–31.

[47] M. C. Jones, ''Variable kernel density estimates and variable kernel density estimates,'' *Austral. J. Statist.*, vol. 32, no. 3, pp. 361–371, Sep. 1990.

[48] J. Y. Hua, D. H. Yuan, G. Li, and L. M. Meng, ''Accurate estimation of Doppler shift in mobile communications with high vehicle speed,'' *Int. J. Commun. Syst.*, vol. 27, no. 12, pp. 3515–3525, Dec. 2014.

[49] G. L. Stüber and G. L. Steuber, *Principles of Mobile Communication*, vol. 2. Springer, 2001.

[50] M. J. Neely, ''Stochastic network optimization with application to communication and queueing systems,'' *Synth. Lectures Commun. Netw.*, vol. 3, no. 1, pp. 1–211, Jan. 2010.

[51] T. Schipper, J. Fortuny-Guasch, D. Tarchi, L. Reichardt, and T. Zwick, ''RCS measurement results for automotive related objects at 23– 27 GHz,'' in *Proc. 5th Eur. Conf. Antennas Propag. (EUCAP)*, Apr. 2011, pp. 683–686.

[52] Y. Wu and J. Feng, ''Development and application of artificial neural network,'' *Wireless Pers. Commun.*, vol. 102, no. 2, pp. 1645–1656, Sep. 2018.

[53] M. Ahmed, R. Seraj, and S. M. S. Islam, ''The *k*-means algorithm: A comprehensive survey and performance evaluation,'' *Electronics*, vol. 9, no. 8, p. 1295, Aug. 2020.

WESAM AL AMIRI (Member, IEEE) received the B.S. degree in communication engineering from Al-Balqa Applied University, Amman, Jordan, in 2014, and the M.S. degree in electrical and computer engineering from Tennessee Technological University, Cookeville, TN, USA, in 2019, where he is currently pursuing the Ph.D. degree with the Department of Electrical and Computer Engineering. His research interests include integrated sensing and communication (ISAC), 5G and beyond, signal processing, and networks security.

TERRY N. GUO (Senior Member, IEEE) received the M.S. degree in telecommunications engineering from Beijing University of Posts and Telecommunications, Beijing, in 1990, and the Ph.D. degree in communications and electronic systems from the University of Electronic Science and Technology of China, Chengdu, in 1997. From January 1997 to December 1999, he was a Postdoctoral Researcher with the University of California, San Diego, advised by Dr. Larry Milstein. In 2000, he worked for a few technology companies in New Jersey. Since 2004, he has been with Tennessee Technological University, Tennessee, where he is currently a Research Professor. He has more than 25 years of industrial and academic experience in wireless communications, data and information science, and RF systems. He has authored/coauthored more than 100 peer-reviewed articles, and has done analytical work and complex proof-of-concept prototyping in many projects. His recent research interests include joint communication and sensing (JC&S) or integrated sensing and communication (ISAC), 5G and beyond, the industrial IoT, and cyber-physical systems (CPS) security.

ALLEN B. MACKENZIE (Senior Member, IEEE) joined Tennessee Tech as the Chairperson of the Department of Electrical and Computer Engineering, in August 2019. Prior to joining Tennessee Tech, he was a Professor with the Department of Electrical and Computer Engineering, Virginia Tech, where he was a Faculty Member, from 2003 to 2019, and where he was the Associate Director of Wireless @ Virginia Tech. From 2012 to 2013, he was an E. T. S. Walton VisitingProfessorwiththeTrinityCollegeDublin.HeiscurrentlytheInterim Associate Dean for Research with Tennessee Tech's College of Engineering. He is the author of more than 90 refereed conference and journal papers and a coauthor of the book *Game Theory for Wireless Engineers*. His research focuses on wireless communications systems and networks. His past and current research sponsors include the National Science Foundation, Science Foundation Ireland, the Defense Advanced Research Projects Agency, and the National Institute of Justice. His current research interests include integration of millimeter wave technology into networks, cognitive radio and cognitive network architectures, and the analysis of wireless systems and networks using game theory and stochastic optimization.

He is a member of the ASEE and ACM. He was previously on the Editorial Boards of IEEE TRANSACTIONS ON COGNITIVE COMMUNICATIONS AND NETWORKING, IEEE TRANSACTIONS ON COMMUNICATIONS, and IEEE TRANSACTIONS ON MOBILE COMPUTING. He was a member of the U.S. Department of Commerce's Spectrum Management Advisory Committee (CSMAC), from 2016 to 2018.